

Plasmonic Helicity-Controlled Conic Metasurface

Yanjun Bao, Shuai Zu, Wei Liu, Xing Zhu, and Zheyu Fang*

School of Physics, State Key Lab for Mesoscopic Physics, Peking University, Beijing 100871,
China

*Email: zhyfang@pku.edu.cn

Conic sections as the oldest known curves in mathematics, play an important role in various areas, such as astronomy, engineering and architecture. Here, we apply conic sections into the optical spin-controlled plasmonic metasurface, which is dependent upon the helicity of the circularly polarized (CP) light. An elliptical metasurface was demonstrated to focus the CP light with opposite helicity into its two foci individually, while the CP light with one certain helicity could be focused into both foci of a hyperbolic metasurface at the same time. Such helicity-dependent behavior is attributed to different geometric phases when CP light with opposite spin interacts with a subwavelength nanoslit. Our configuration provides a route for spin-based plasmonic device design and opens up a new realm for the application of traditional conic sections.

Metasurfaces, artificially subwavelength-structured interfaces, are able to control the phase of light, leading to versatile optical functionalities, such as anomalous refraction and reflection¹⁻⁵, vortex beam generation⁵⁻⁷, and optical holography⁸⁻¹⁴, etc. In order to achieve a desired functionality, the spatial shape and size of each unit cell

should be precisely designed. Nanoslit as one of the most commonly used optical elements, offers a flexible way to manipulate the light due to its orientation-dependent geometric phase under circularly polarized (CP) light excitation¹⁵⁻¹⁷. With this flexibility, some optical spin related applications that depend upon the helicity of the CP light have been realized, such as optical spin-Hall effect¹⁵, and tunable directional propagation of surface plasmon polaritons (SPPs)^{16,17}.

Conic sections are the oldest curves that have been studied rigorously and applied widely in mathematics, physics, and astronomy, etc. The circle, ellipse, parabola and hyperbola as four types of conic sections, are determined by the angle at which a plane intersects with a right circular cone (Fig. 1a)¹⁸. Circular nanostructures are the most commonly used conic sections for the plasmonic focusing when the structure was illuminated with linearly^{19,20} and radially polarized lights^{21,22}. It is interesting to note that the ellipse and hyperbola also have fascinating reflective properties in geometric optics, for example, light emanating from a focus of an elliptical mirror can be reflected by the ellipse structure and propagates into the second one (Fig. 1b), while for a hyperbolic mirror, light directed towards at a focus can be reflected to the other one (Fig. 1c). Thus, it is expected that a designed metasurface with conic section shapes (Fig. 1d,e) may have interesting properties to realize the control of CP light at nanoscale.

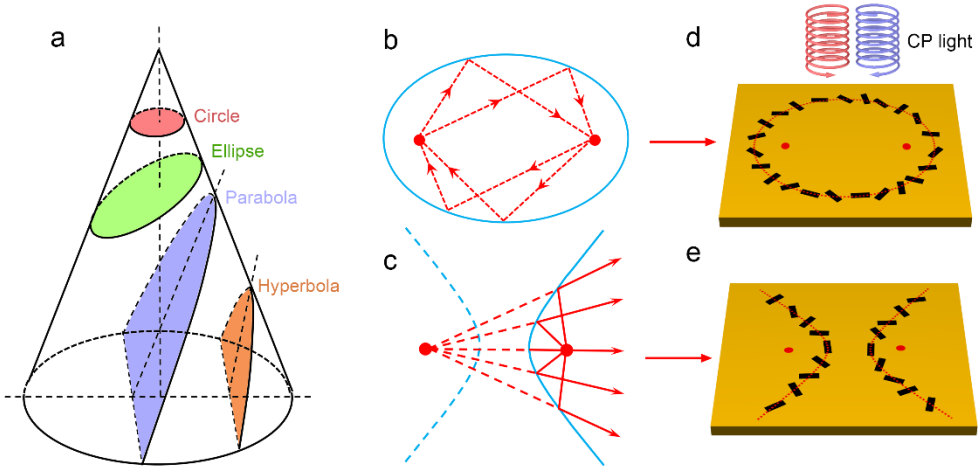


Figure 1 | From conic sections to conic metasurfaces. (a) A conic section is formed by the intersection of a plane with a right circular cone. Circle: the plane is perpendicular to the axis of the cone; Ellipse: the plane is inclined with an angle, but still cuts through the whole surface of the cone; Parabola: the plane is parallel to a generator of the cone; Hyperbola: the plane is inclined at a small angle to the axis of the cone, resulting in an open curve. (b,c) Reflective properties of elliptical and hyperbolic mirrors. (b) Light emanating from a focus of ellipse is reflected to the second one. (c) Light directed towards at a focus of hyperbola is reflected to the other one. (d,e) Schematic of an elliptical (d) and hyperbolic metasurface (e) that composed of metallic nanoslits illuminated by the CP light.

Here, for the first time, we proposed plasmonic metasurfaces with such conic section shapes for helicity-controlled SPP focusing, where the elliptical metasurface was used to focus the CP light with opposite helicity into two foci individually, and the hyperbolic metasurface was used to focus the CP light with one certain helicity at its both foci simultaneously. Our conic metasurfaces were further modified for working at different wavelengths at the same time. The optical spin-dependent SPP

propagation control was verified experimentally by using scanning near-field optical microscopy (SNOM), which has a good agreement with our theoretical prediction.

Results

Phase of SPPs from a nanoslit to an arbitrary point. Plasmonic nanoslit structure was perforated in an Au film (Fig. 2a), which was used to generate SPPs preferentially when the normal incident light is polarized perpendicular to its long axis. The SPP emission pattern is approximately that of an in-plane point dipole²³, which is shown in Fig. 2b. Considering a point $F_1 (x_1, y_1)$ located a distance r_1 from the nanoslit $O (x, y)$ (Fig. 2a), the phase of SPPs from the nanoslit O to the point F_1 can be expressed by

$$\psi = \psi_a + \psi_g + 2\pi r_1 / \lambda_{spp}. \quad (1)$$

The first term ψ_a is the antisymmetric phase. As shown in Fig. 2b, the radiated SPP field (\mathbf{E}_a) exhibits an anti-phase pattern relative to the long axis of the nanoslit. For a general nanoslit with an azimuth angle φ (between 0 and π) along the x -axis, SPPs propagating away toward two sides of the long axis (dashed red line in Fig. 2a) have a π phase difference between them, which can be mathematically written as

$$\psi_a = \begin{cases} 0 & \text{if } \varphi < \beta < \varphi + \pi \\ \pi & \text{if } \varphi - \pi < \beta < \varphi \end{cases} \quad (2)$$

where $\beta = \text{atan2} (y_1 - y, x_1 - x)$ is the orientation angle of vector OF_1 . The second term in equation (1) is the geometric phase. Because only the incident polarization perpendicular to the long axis of the nanoslit can efficiently excite SPPs, the geometric phase is $\psi_g = \sigma\varphi$, where $\sigma = \pm 1$ corresponding to the helicity of the right (RCP) and left (LCP) circularly polarized light. The third term $2\pi r_1 / \lambda_{spp}$ is the

phase retardation of SPPs propagating from O to F_1 , where λ_{spp} is the SPP wavelength. The nanoslit-orientation-dependent phase provides us an easy way and an extra degree of freedom to control the CP light with significant flexibility.

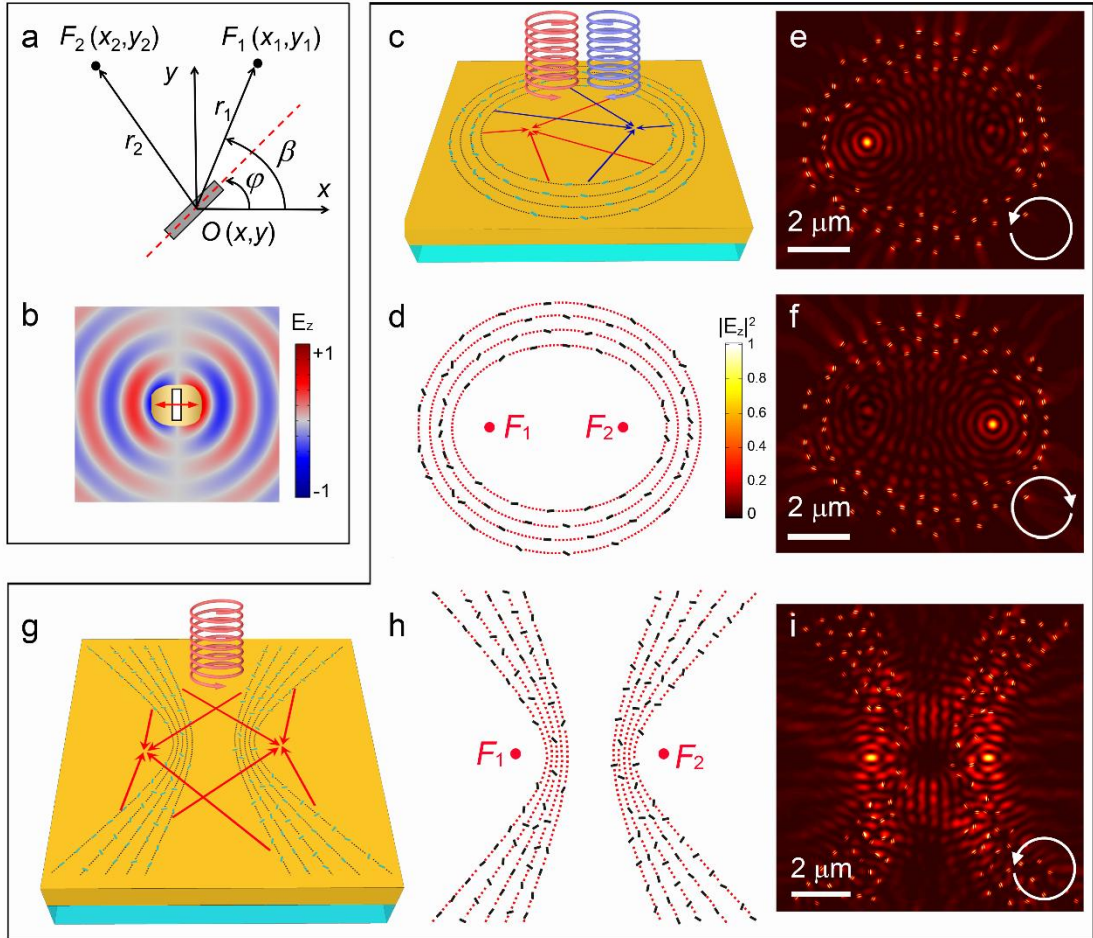


Figure 2 | Design of conic metasurfaces. (a) Two points $F_1(x_1, y_1)$ and $F_2(x_2, y_2)$ located a distance of r_1 and r_2 from a nanoslit $O(x, y)$ with an azimuth angle φ , respectively. The red dashed line indicates the long axis of the nanoslit. (b) The calculated normal component of the SPP electric field \mathbf{E}_z launched by a nanoslit that is perforated in an Au film when the incident light is polarized perpendicular to its long axis (polarization indicated by a red arrow). (c,d) Schematic (c) and top view (d) of an elliptical metasurface that the LCP (RCP) incident light is focused at the

left (right) focus of the ellipse. (e,f) FDTD simulated near-field intensity $|\mathbf{E}_z|^2$ of the elliptical metasurface with the illumination of LCP (e) and RCP (f) incidences. (g,h) Schematic (g) and top view (h) of a hyperbolic metasurface that the LCP incidence is focused at two foci of the hyperbola simultaneously. In d and h, the black solid rectangles represent nanoslits and dashed red lines indicate traces of conic sections. (i) FDTD simulated near-field intensity $|\mathbf{E}_z|^2$ of the hyperbolic metasurface with the illumination of LCP.

Design of conic metasurface for helicity-controlled SPPs. As the first example, we assume that SPPs can be focused at positions $F_1(x_1, y_1)$ and $F_2(x_2, y_2)$ for LCP and RCP incident lights, respectively (Fig. 2b). By requiring two constructive conditions at these two points, we can determine the coordinate of each nanoslit by following equation (Supplementary Section 1),

$$r_1 + r_2 = \left[k - \frac{\psi_a(x, y, x_1, y_1) + \psi_a(x, y, x_2, y_2)}{2\pi} + \varphi_0 \right] \lambda_{spp} \quad (3)$$

where $r_1(r_2)$ is the distance between point $F_1(F_2)$ and the center of nanoslit O , k is an integer and φ_0 is a constant value. Because $\psi_a(x, y, x_{1(2)}, y_{1(2)})$ is either 0 or π , the second term on the right side in the bracket of equation (3) is either 0, 0.5 or 1. Once the position (r_1 and r_2) is determined, the azimuth angle of nanoslit can be calculated (Supplementary Section 1). It is clearly to see that the position of nanoslit is located on the trajectory of an ellipse with two foci at points F_1 and F_2 .

When the two constructive conditions are applied to CP light with one certain helicity (for example, LCP), the incident light can be focused at points F_1 and F_2 simultaneously, and one can obtain (Supplementary Section 1)

$$r_1 - r_2 = \left[k - \frac{\psi_a(x, y, x_1, y_1) - \psi_a(x, y, x_2, y_2)}{2\pi} + \varphi_0 \right] \lambda_{spp} \quad (4)$$

where the parameters have the same meanings as those in equation (3). The second term on the right side in the bracket of above equation is either -0.5, 0 or 0.5. Equation (4) indicates a hyperbolic curve with two foci at points F_1 and F_2 .

Figure 2c,d show our designed elliptical metasurface, which is able to focus CP light with opposite helicity into two foci of the ellipse, individually. While, the hyperbolic metasurface in Fig. 2h,i can focus the LCP incidence at both foci simultaneously (see the design of metasurfaces in Methods). Both structures were designed for operation at wavelength of $\lambda=671$ nm. For a fixed k value in equation (3) and equation (4), the nanoslits may locate at three different traces depending on their orientations and thus are not fully distributed at each trace of conic sections. Finite-difference time-domain (FDTD) simulations were performed and the simulated $|\mathbf{E}_z|^2$ fields are shown in Fig. 2e, f and i. It can be seen that the simulated results show good agreement with our predictions.

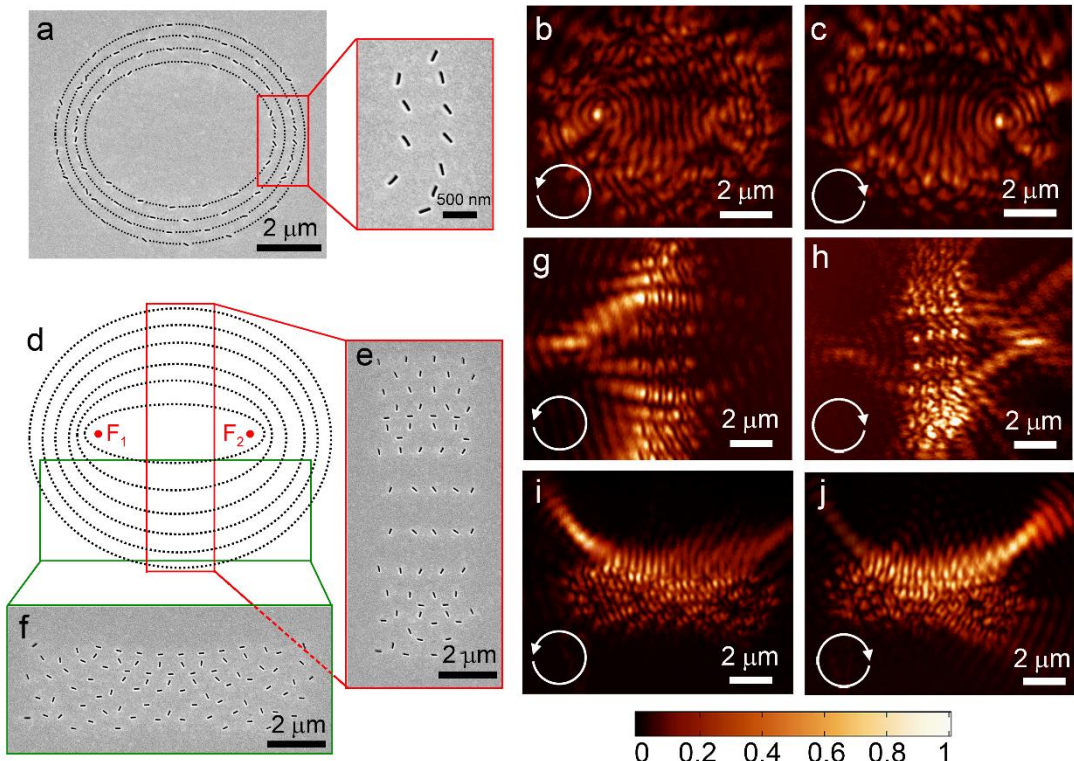


Figure 3 | Experimental demonstration of helicity-controlled SPPs in elliptical metasurface.

(a) SEM images of the elliptical metasurface with low and high magnification. The black dashed lines are a guide for the eye of elliptical traces. **(b,c)** Measured near-field optical intensity profiles for the elliptical metasurface with 671 nm LCP **(b)** and RCP **(c)** excitations. **(d)** Design strategy of metasurfaces with different functionalities. **(e,f)** SEM images of two metasurfaces, which can focus CP light with opposite helicity at each side of structure **(e)** or at the same (upper) side **(f)**. **(g-j)** Measured near-field optical intensities under LCP (left column) and RCP (right column) lights for metasurfaces shown in **e** (upper row) and **f** (lower row).

Experimentally demonstration of helicity-controlled conic metasurface. To experimentally demonstrate the concept, we fabricated conic metasurfaces by using Au electron-beam evaporation and focused ion-beam milling (see Methods). Figure 3a presents a scanning electron microscopy (SEM) image of the fabricated elliptical

metasurface with black dashed lines for the eye guide of elliptical traces. A collection-mode SNOM system was used to measure SPP distributions (see Methods). Figure 3b,c show the measured near-field optical distribution of the elliptical metasurface, which clearly demonstrate that SPPs are focused at F_1 for LCP incidence, and switched to F_2 when the helicity of the incident light is changed to RCP. It is worthy to mention that when the two foci overlap with each other, the ellipse becomes a circle, which can focus the two different CP lights at the same point (Supplementary Section 2 and Fig. S1). It was reported that SPPs under LCP and RCP excitations can be focused at the same side of the distributed nanoslits²⁴ or directionally launched toward to each side¹⁷. Similar functionalities can be easily realized based on our elliptical metasurface. As shown in Fig. 3d, all of the nanoslits located at different elliptical traces (dashed black lines) can focus the SPPs at their common foci (F_1 and F_2). By choosing parts of the elliptical traces, for example, regions between two foci (red rectangle) or below (green rectangle), the resulting metasurface can focus the CP light with opposite helicity at each side or at the same (upper) side. We fabricated the two metasurfaces with their SEM images shown in Fig. 3e,f. The measured SPP intensities under LCP and RCP lights for the two metasurfaces are shown in Fig. 3g-j, which are in good agreements with our theory and the FDTD simulated results (Figs. S2, 3).

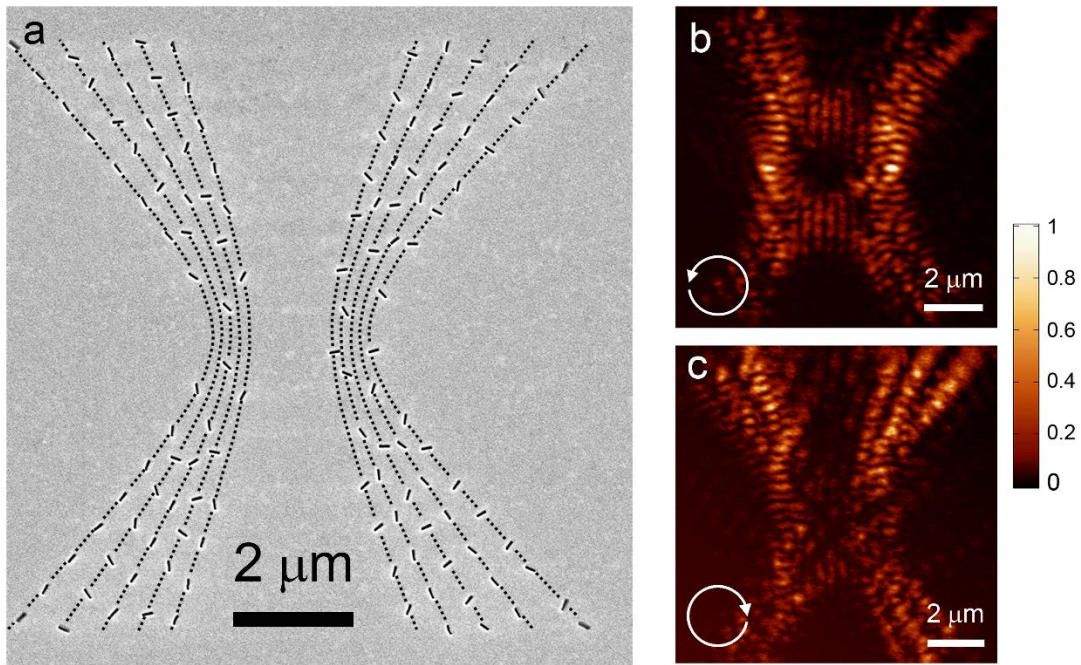


Figure 4 | Experimental demonstration of helicity-controlled SPPs in hyperbolic metasurface.

(a) SEM image of the hyperbolic metasurface with the black dashed lines for the eye guide of hyperbolic traces. **(b,c)** Measured near-field optical intensity profiles under LCP **(b)** and RCP **(c)** light excitation at wavelength of 671 nm.

Figure 4a shows the SEM image of the hyperbolic metasurface according to the structural design in Fig. 2h. The measured intensity with the LCP light illumination is presented in Fig. 4b, and both foci are clearly observed at F_1 and F_2 . For comparison, Fig. 4c shows the experimental result when the metasurface is illuminated with RCP light. The observed two foci in Fig. 4b disappear in this situation, as expected with our simulation (Fig. S4).

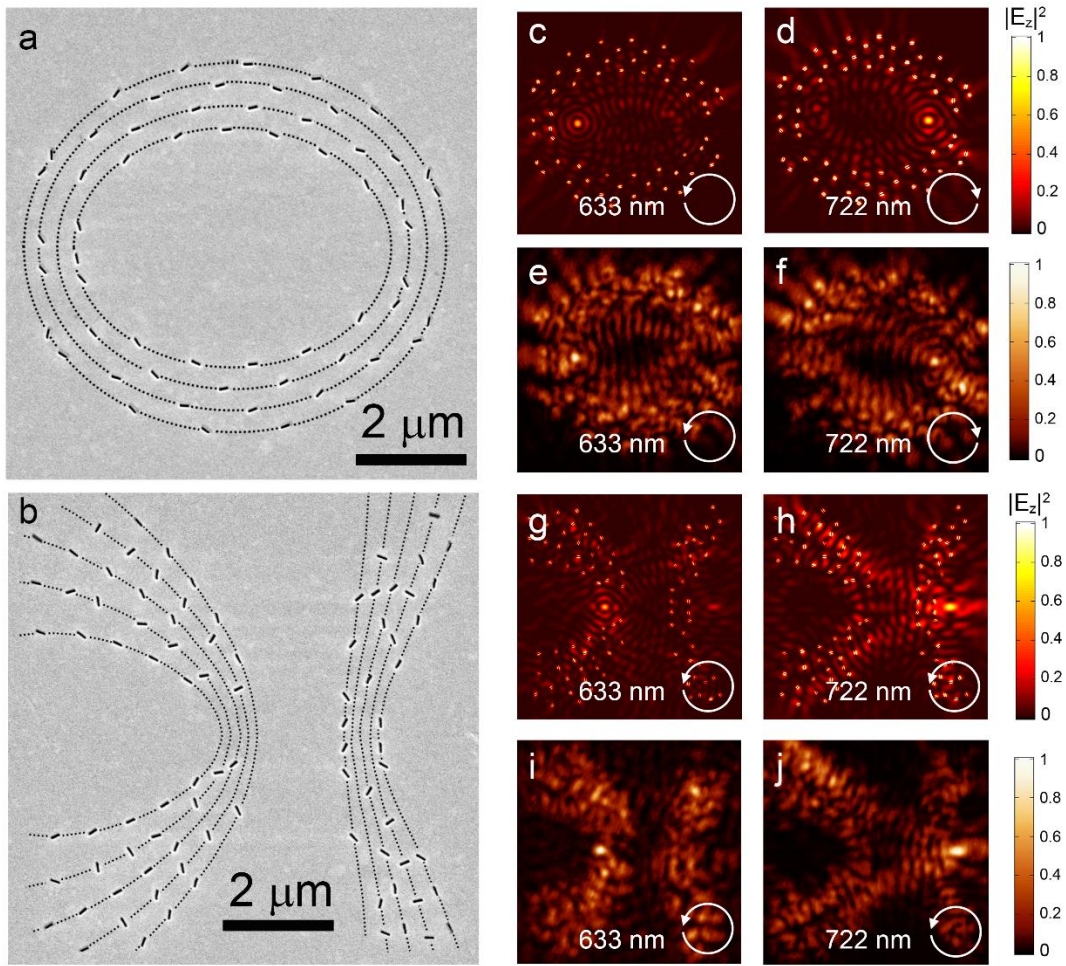


Figure 5 | Conic metasurfaces operating at two wavelengths simultaneously. (a,b) SEM images of the modified elliptical (a) and hyperbolic (b) metasurfaces with the black dashed lines for the eye guide. (c-f) Simulated (upper row) and experimental (lower row) results for the modified elliptical metasurface under LCP incidence with wavelength of 633 nm (left column) and RCP incidence with wavelength of 722 nm (right column). (g-j) Simulated (upper row) and experimental (lower row) results for the modified hyperbolic metasurface under LCP incidences with wavelength 633 nm (left column) and 722 nm (right column). The operating wavelengths and the helicity of incident light are indicated in each panel.

The above conic metasurfaces can be further modified with the two constructive conditions at points F_1 and F_2 operating at different incident wavelengths (Supplementary Section 3). Figure 5a,b show the modified elliptical (Fig. 5a) and hyperbolic (Fig. 5b) metasurfaces with $\lambda_1=633$ nm and $\lambda_2=722$ nm. The trajectory of Fig. 5a shows similar but not exact the same pattern as an ellipse, while the one in Fig. 5b looks similar to a hyperbola but with two asymmetric branches. For the modified elliptical metasurface, both the simulations and experiments (Fig. 5c-f) show that a focus can be observed at point F_1 for LCP incidence with wavelength of 633 nm, and a focus at F_2 for RCP incidence with wavelength of 722 nm. As for the modified hyperbolic metasurface, the incident LCP lights at wavelengths of 633 and 722 nm are focused at positions F_1 and F_2 , respectively (Fig. 5g-j).

Discussion

In summary, we proposed and experimentally demonstrated a novel scheme for the generation of helicity-controlled surface plasmons in conic section shape nanostructures. Based on the flexible geometric phase of nanoslit, we designed two metasurfaces with elliptical and hyperbolic shapes, and demonstrated that the helicity of incident CP light is associated with their foci in different ways. For the elliptical metasurface, LCP and RCP lights could be focused at each of its two foci, while for the hyperbolic metasurface, CP light with one certain helicity could be focused at the two foci simultaneously. The conic metasurfaces were further modified for working at two different wavelengths at the same time. We believe that our concept presented

here opens up a new realm for the application of traditional conic sections and may be used in a wide range of fields such as spin-based nanophotonics, plasmonic wavelength demultiplexer and focusing.

Methods

Numerical Simulations. The numerical simulation was performed by using a finite-difference time-domain (FDTD) commercial software package (Lumerical). The perfect matched layers (PMLs) boundary condition was used to suppress spurious numerical reflections. The permittivity of Au is obtained from the experimental data in literature²⁵ and the refractive index of glass is set to be 1.45. The electric fields were obtained by monitors at 10 nm above the Au film.

Design of metasurfaces. For the metasurfaces shown in Figs. 2, 4, 5 and 3a, the locations of foci are designed at F_1 (-2 μm , 0 μm) and F_2 (2 μm , 0 μm), respectively. For the metasurfaces shown in Fig. 3e,f, the foci are F_1 (-5 μm , 0 μm) and F_2 (5 μm , 0 μm), respectively. The geometrical parameters of the nanoslit are identical with width of $w = 50$ nm and length of $L=200$ nm. The distance between two adjacent nanoslits has a minimum gap of 300 nm to avoid structural overlapping.

Sample fabrication and optical measurements. We evaporated 100 nm thickness Au film onto a glass substrate and used focused ion beam (FIB) milling to etch the nanoslit structures on the film. The evaporation rate was 0.5 \AA s^{-1} and the beam current was 1.1 pA to ensure the fabrication accuracy. A commercial NSOM system (Nanonics Imaging Multiview 1000) was used to measure

the SPP distributions. The probe is metal-coated, tapered fiber probe with an aperture at the facet. The probe was modified with sharp perturbation to increase the coupling efficiency of the E_z component. In addition, because the E_z component of SPPs is much larger than the in-plane E_{x-y} component at the Au surface, the measured optical intensity is expected mostly come from the normal electric field $|E_z|^2$. The samples were back-illuminated with circular polarized light, which is generated by a quarter wave plate and a polarizer. Three lasers with different wavelengths at 633, 671 and 722 nm were used as the excitation sources. Figure S5 presents a full schematic of the experimental setup.

ACKNOWLEDGEMENTS

This work is supported by National Science Foundation of China (Grant No. 61422501, 11374023, and 61521004), the National Basic Research Program of China (973 Program, Grant No. 2015CB932403), Beijing Natural Science Foundation (Grant No. L140007), and Foundation for the Author of National Excellent Doctoral Dissertation of PR China (Grant No.201420), and National Program for Support of Top-notch Young Professionals.

Author contributions

Y. Bao and Z. Fang conceived the idea, Y. Bao designed the metasurfaces and performed the simulation. Y. Bao, S. Zhu, W. Liu did the experiments. All authors discussed the results and wrote the manuscript.

Additional information

Supplementary information is available in the online version of the paper. Reprints and permission information is available online at <http://www.nature.com/reprints>. Correspondence and requests for materials should be addressed to Z. F.

Competing financial interests

The authors declare no competing financial interests.

References

1. N. F. Yu and F. Capasso, Flat optics with designer metasurfaces. *Nat. Mater.* **13**, 139-150 (2014).
2. L. Liu et al., Broadband metasurfaces with simultaneous control of phase and amplitude. *Adv. Mater.* **26**, 5031-5036 (2014).
3. Z. Li, E. Palacios, S. Butun and K. Aydin, Visible-frequency metasurfaces for broadband anomalous reflection and high-efficiency spectrum splitting. *Nano Lett.* **15**, 1615-1621 (2015).
4. S. Sun et al., High-efficiency broadband anomalous reflection by gradient meta-surfaces. *Nano Lett.* **12**, 6223-6229 (2012).
5. N. Yu et al., Light propagation with phase discontinuities: generalized laws of reflection and refraction. *Science* **334**, 333-337 (2011).
6. L. Huang et al., Dispersionless phase discontinuities for controlling light propagation. *Nano Lett.* **12**, 5750-5755 (2012).
7. Y. M. Yang et al., Dielectric Meta-Reflectarray for Broadband Linear Polarization Conversion and Optical Vortex Generation. *Nano Lett.* **14**, 1394-1399 (2014).
8. W. T. Chen et al., High-Efficiency Broadband Meta-Hologram with Polarization-Controlled Dual Images. *Nano Lett.* **14**, 225-230 (2014).
9. X. J. Ni, A. V. Kildishev and V. M. Shalaev, Metasurface holograms for visible light. *Nat. Commun.* **4**, 2807 (2013).
10. L. Huang et al., Three-dimensional optical holography using a plasmonic metasurface. *Nat. Commun.* **4**, 2808 (2013).
11. D. Wintz, P. Genevet, A. Ambrosio, A. Woolf and F. Capasso, Holographic Metalens for Switchable Focusing of Surface Plasmons. *Nano Lett.* **15**, 3585-3589 (2015).
12. Y. Yifat et al., Highly Efficient and Broadband Wide-Angle Holography Using Patch-Dipole Nanoantenna Reflectarrays. *Nano Lett.* **14**, 2485-2490 (2014).
13. G. X. Zheng et al., Metasurface holograms reaching 80% efficiency. *Nat. Nanotechnol.* **10**, 308-312 (2015).
14. D. D. Wen et al., Helicity multiplexed broadband metasurface holograms. *Nat. Commun.* **6**, 8241 (2015).
15. S. Xiao, F. Zhong, H. Liu, S. Zhu and J. Li, Flexible coherent control of plasmonic spin-Hall effect.

Nat. Commun. **6**, 8360 (2015).

16. J. Lin et al., Polarization-controlled tunable directional coupling of surface plasmon polaritons. *Science* **340**, 331-334 (2013).
17. L. Huang et al., Helicity dependent directional surface plasmon polariton excitation using a metasurface with interfacial phase discontinuity. *Light Sci. Appl.* **2**, e70 (2013).
18. V. J. Katz, *A history of mathematics : an introduction*, Addison-Wesley, 1998.
19. F. López-Tejeira et al., Efficient unidirectional nanoslit couplers for surface plasmons. *Nat. Phys.* **3**, 324-328 (2007).
20. Z. Fang et al., Plasmonic focusing in symmetry broken nanocorral. *Nano Lett.* **11**, 893-897 (2011).
21. G. M. Lerman, A. Yanai and U. Levy, Demonstration of Nanofocusing by the use of Plasmonic Lens Illuminated with Radially Polarized Light. *Nano Lett.* **9**, 2139-2143 (2009).
22. W. B. Chen, D. C. Abeyasinghe, R. L. Nelson and Q. W. Zhan, Plasmonic Lens Made of Multiple Concentric Metallic Rings under Radially Polarized Illumination. *Nano Lett.* **9**, 4320-4325 (2009).
23. T. Tanemura et al., Multiple-wavelength focusing of surface plasmons with a nonperiodic nanoslit coupler. *Nano Lett.* **11**, 2693-2698 (2011).
24. S. Y. Lee, K. Kim, G. Y. Lee and B. Lee, Polarization-multiplexed plasmonic phase generation with distributed nanoslits. *Opt. Express* **23**, 15598-15607 (2015).
25. P. B. Johnson and R. W. Christy, Optical Constants of the Noble Metals. *Phys. Rev. B* **6**, 4370-4379 (1972).

Supporting Information For

Plasmonic Helicity-Controlled Conic Metasurface

Yanjun Bao, Shuai Zu, Wei Liu, Xing Zhu, and Zheyu Fang*

School of Physics, State Key Lab for Mesoscopic Physics, Peking University, Beijing 100871,
China

*Email: zhyfang@pku.edu.cn

Contents:

Supplementary Section 1: Deviation of the trace equation of the elliptical and hyperbolic metasurfaces.

Supplementary Section 2: Circular metasurface for focusing both LCP and RCP lights at its center.

Supplementary Section 3: Deviation of the trace equation of the modified elliptical and hyperbolic metasurfaces.

Figure S1: Circular metasurface for focusing both CP lights at its center.

Figure S2: Metasurface for focusing CP lights with opposite helicity at its each side.

Figure S3: Metasurface for focusing CP lights with opposite helicity at its same side.

Figure S4: Simulated and experimental optical intensities of hyperbolic under RCP incident light.

Figure S5: NSOM setup for measurement of the near field intensity.

1-Deviation of the trace equation of the elliptical and hyperbolic metasurfaces

If the generated SPPs from a nanoslit with an orientation angle of φ can be focused at positions $F_1(x_1, y_1)$ and $F_2(x_2, y_2)$ for LCP incidence and RCP incidence with wavelength of λ , respectively, we can determine the coordinates and orientation angles of nanoslits as follows by requiring constructive interference at the two points,

$$\begin{aligned} -\varphi + \psi_a(x, y, x_1, y_1) + 2\pi r_1 / \lambda_{spp} &= 2m\pi + \varphi_1 && \text{for LCP} \\ \varphi + \psi_a(x, y, x_2, y_2) + 2\pi r_2 / \lambda_{spp} &= 2n\pi + \varphi_2 && \text{for RCP} \end{aligned} \quad (\text{S1})$$

where $r_1(r_2)$ is the distance between point $F_1(F_2)$ and the center of nanoslit O , m (n) are integers, $\varphi_1(\varphi_2)$ are two constant values and λ_{spp} is the SPP wavelength for incident light wavelength λ . By adding the two equations in Eq. S1, we obtain

$$r_1 + r_2 = \left[k - \frac{\psi_a(x, y, x_1, y_1) + \psi_a(x, y, x_2, y_2)}{2\pi} + \varphi_0 \right] \lambda_{spp} \quad (\text{S2})$$

where k is an arbitrary integer and $\varphi_0 = \frac{\varphi_1 + \varphi_2}{2\pi}$. The above equation shows an

elliptical trace with two foci at F_1 and F_2 (Eq. 3 in the main text).

If we apply the two constructive conditions (Eq. S1) to the CP light with one certain helicity (for example, LCP), and the light can be focused at points F_1 and F_2 at the same time, one can obtain

$$\begin{aligned} -\varphi + \psi_a(x, y, x_1, y_1) + 2\pi r_1 / \lambda_{spp} &= 2m\pi + \varphi_1 \\ -\varphi + \psi_a(x, y, x_2, y_2) + 2\pi r_2 / \lambda_{spp} &= 2n\pi + \varphi_2 \end{aligned} \quad (\text{S3})$$

By subtracting these two equations from each other, we get an equation that determines the coordinates of nanoslits as follows,

$$r_1 - r_2 = \left[k - \frac{\psi_a(x, y, x_1, y_1) - \psi_a(x, y, x_2, y_2)}{2\pi} + \varphi_0 \right] \lambda_{spp} \quad (\text{S4})$$

where $\varphi_0 = \frac{\varphi_1 - \varphi_2}{2\pi}$. The above equation shows a hyperbolic trace with two foci at F_1 and F_2 (Eq. 4 in the main text).

2- Circular metasurface for focusing both LCP and RCP lights at its center

For the elliptical metasurface (Eq. S2), when the two foci overlap with each other, the ellipse becomes a circle with a radius of

$$r = \left[\frac{k}{2} + \frac{\varphi_0}{2} - \frac{\psi_a(x, y, x_1, y_1)}{2\pi} \right] \lambda_{spp} \quad (\text{S5})$$

and the azimuthal angles of all nanoslits are the same, as being

$$\varphi = (\varphi_2 - \varphi_1) / 2 \quad (\text{S6})$$

Figure S1a shows the structure of such a circular metasurface with $\varphi_0 = 0$. The simulated electric field intensities for LCP and RCP incidences are shown in Fig. S1b-c, which indicates that both polarizations are focused at the center of the structure.

3-Deviation of the trace equation of the modified elliptical and hyperbolic metasurfaces

For the above elliptical and hyperbolic metasurfaces, the two constructive conditions (Eq. S1 and Eq. S3) have the same operating wavelengths. When they are different, such metasurfaces can work at two wavelengths simultaneously. For this situation, the two constructive conditions of the elliptical metasurface become as

$$-\varphi + \psi_a(x, y, x_1, y_1) + 2\pi r_1 / \lambda_{spp1} = 2m\pi + \varphi_1 \quad \text{for LCP}$$

$$\varphi + \psi_a(x, y, x_2, y_2) + 2\pi r_2 / \lambda_{spp2} = 2n\pi + \varphi_2 \quad \text{for RCP} \quad (S7)$$

where λ_{spp1} and λ_{spp2} are the SPP wavelengths of the different incident lights at wavelengths λ_1 and λ_2 , respectively. By adding the two equations in Eq. S7, we obtain

$$r_1 / \lambda_{spp1} + r_2 / \lambda_{spp2} = k + \frac{\varphi_1 + \varphi_2}{2\pi} - \frac{\psi_a(x, y, x_1, y_1) + \psi_a(x, y, x_2, y_2)}{2\pi} \quad (S8)$$

where k is an arbitrary integer. For such a modified elliptical metasurface with its equation trace obeying Eq. S8, the LCP light with wavelength λ_1 can be focused at point F_1 and the RCP light with wavelength λ_2 can be focused at position F_2 . Figure 5a of the main text shows a SEM image of the modified elliptical metasurface with $\lambda_1=633$ nm and $\lambda_2=722$ nm.

As for the hyperbolic metasurface, the two constructive conditions become as

$$\begin{aligned} -\varphi + \psi_a(x, y, x_1, y_1) + 2\pi r_1 / \lambda_{spp1} &= 2m\pi + \varphi_1 \\ -\varphi + \psi_a(x, y, x_2, y_2) + 2\pi r_2 / \lambda_{spp2} &= 2n\pi + \varphi_2 \end{aligned} \quad (S9)$$

By subtracting the two equations from each other, we have

$$r_1 / \lambda_{spp1} - r_2 / \lambda_{spp2} = k + \frac{\varphi_1 - \varphi_2}{2\pi} - \frac{\psi_a(x, y, x_1, y_1) - \psi_a(x, y, x_2, y_2)}{2\pi} \quad (S10)$$

The modified hyperbolic metasurface is thus able to focus the LCP incidences with wavelengths λ_1 and λ_2 at points F_1 and F_2 , respectively. Figure 5b of the main text shows a SEM image of the modified hyperbolic metasurface with $\lambda_1=633$ nm and $\lambda_2=722$ nm.

Figures

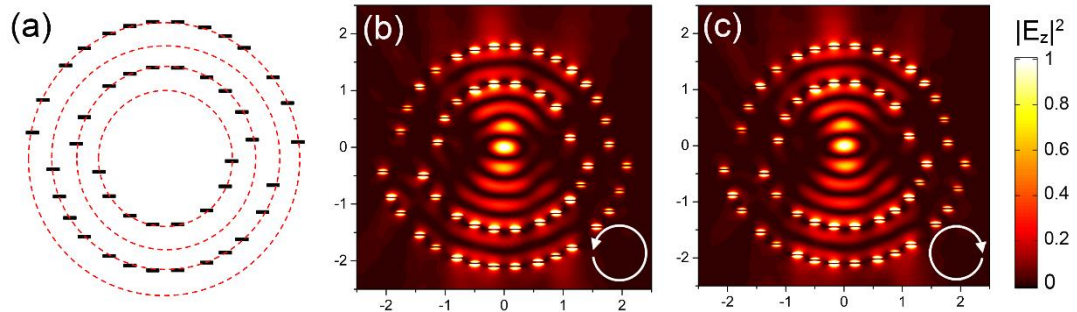


Figure S1 (a) The geometric pattern of the circular metasurface, where the black rectangles represent the nanoslits and the dashed red lines indicate the circular traces. (b-c) The simulated near-field intensities with the illumination of LCP (b) and RCP (c) incidences.

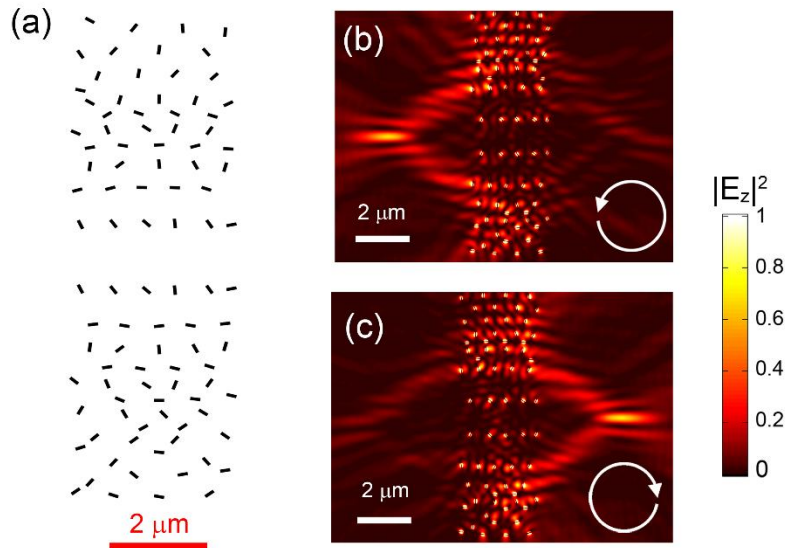


Figure S2 (a) The design pattern of the metasurface that can focus the CP light with opposite helicity at each side of it. (b-c) The simulated near-field intensities with the illumination of LCP (b) and RCP (c) incidences.

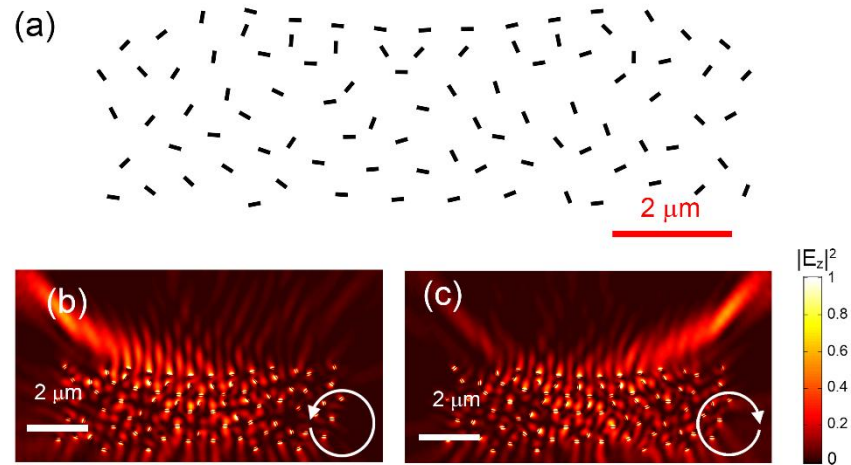


Figure S3 (a) The design pattern of the metasurface that can focus the CP light with opposite helicity at the same side of it. (b-c) The simulated near-field intensities with the illumination of LCP (b) and RCP (c) incidences.

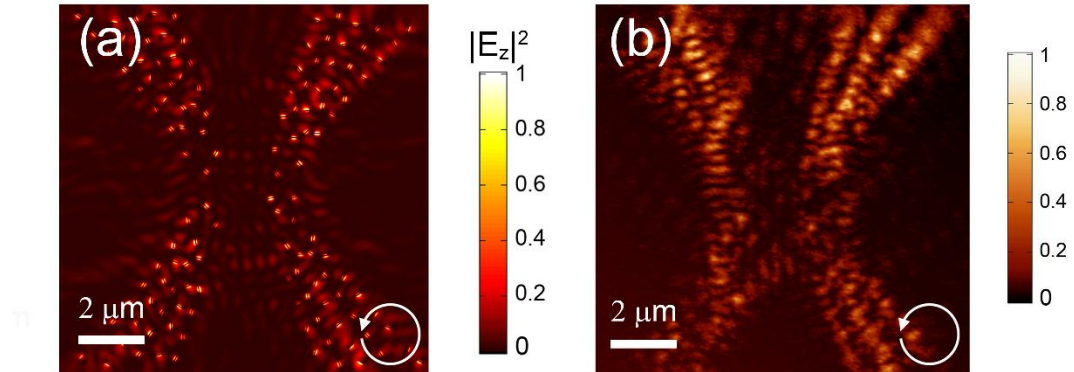


Figure S4 Simulated (a) and measured (b) electric field intensities of the hyperbolic metasurface with RCP incident light. It can be seen that there are no foci for this situation.

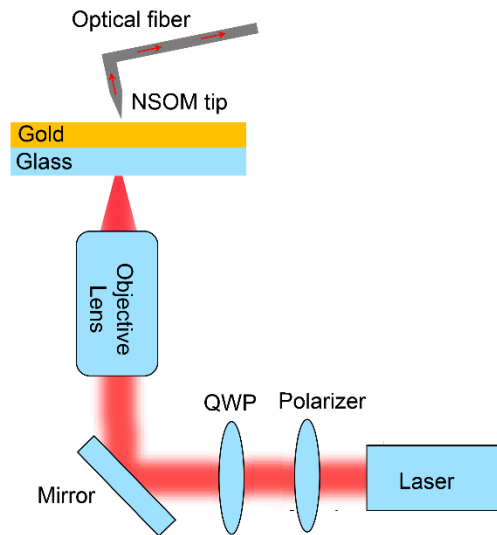


Figure S5 NSOM setup for measurement of the near field intensity. The samples were back-illuminated with circular polarized light, which is generated by a quarter wave plate (QWP) and a polarizer.